Diagnostic for phases and quantum critical regions using deviations from the local fluctuation-dissipation theorem

E. Duchon, Y. Kato, and N. Trivedi

Phys. Rev. A **86**, 063608 — Published 6 December 2012

DOI: 10.1103/PhysRevA.86.063608

Diagnostic for Phases and Quantum Critical Regions using Deviations from the Local Fluctuation-Dissipation Theorem

E. Duchon[1], Y. Kato[2], and N. Trivedi[1]
[1] *Department of Physics, Ohio State University, Columbus, Ohio 43210, USA and*
[2] *Theoretical Division, Los Alamos National Laboratory, Los Alamos, New Mexico 87545 USA*

We propose that the temperature dependence of a single quantity $R = \kappa_i/\delta n_i^2$, the ratio of the local compressibility to the local number fluctuations, can be used to map out the finite temperature phase diagram, diagnose the critical region around a quantum phase transition, and identify critical points belonging to different universality classes. We test our proposal using state-of-the-art large-scale quantum Monte Carlo simulations of the two-dimensional Bose Hubbard model. Our results have implications for recently developed single site imaging experiments.

I. INTRODUCTION

Quantum phase transitions are dramatic events where quantum fluctuations drive one ground state into an entirely different ground state upon tuning a parameter in the Hamiltonian. These phenomena are observed in condensed matter systems and ultracold atomic gases and are even relevant to the quantum fluctuations that give birth to galaxies. Quantum gases in optical lattices emulate Fermi[1–7] and Bose[8, 9] Hubbard models and offer a unique platform to study quantum phases and the phase transitions between them since the tuning parameter t/U, the tunneling t of an atom from one well to the next relative to the interaction U between atoms, can be easily tuned by varying the laser intensity and magnetic fields[10]. Not only are these phases with their associated excitations interesting, but the quantum critical point (QCP) that exists at zero temperature and at a special value of t/U leaves a definite footprint in the thermodynamics and response functions for a large range of finite temperatures. This quantum critical region is dominated by large fluctuations arising from the new degrees of freedom that must form as the system transits from one phase to the other[11]. Here we focus on identifying this region using fundamental thermodynamic relations. Theoretical investigations around the quantum critical point, which occurs at t/U of order unity, remain extremely challenging because of the absence of a small parameter.

For the Bose Hubbard model (BHM), the detection and characterization of the superfluid and insulating phases has been inferred from four primary classes of experiments: (a) Momentum distribution function obtained from time-of-flight observations of the expanding clouds[9, 12–14]; (b) Energy gap of the Mott phase probed by the location of resonances in the excitation spectrum using a potential gradient[9] and excitation spectrum of the superfluid probed using Bragg spectroscopy[15, 16]; (c) Global number fluctuations measured by magnetic resonance imaging techniques to study number squeezing and suppression of spin flipping collisions across the transition and in the Mott state[17]; (d) Time scales required for equilibration in the Mott phase using mass transport measurements[18–21].

In principle, the temperature scales bounding the quantum critical region could be extracted from a combination of the techniques discussed above, but in practice the global nature of these probes makes the information necessary to map the phase diagram from inhomogeneous trapped gases difficult to disentangle.

A new class of experiments have the remarkable capability to probe the atomic gases in optical lattices *in situ* on an atomic scale[19, 20, 22, 23]. These experiments have tremendous potential since they provide spatially-resolved information about each of the phases that exist within a single, inhomogeneous experimental system. These recently developed local microscopic and spectroscopic techniques are ideally suited to probe the large fluctuations across the quantum phase transition. Indeed, several investigations into scaling local quantities to identify the QCPs have been published [24–27].

In this article, we provide the theoretical framework for the application of a local fluctuation-dissipation theorem to experiments to gain fundamental insights into the nature of both gapped and gapless phases, their low-lying excitations and quantum criticality. Motivated by the success of recent experiments to access the local density *in situ*, we define a local dissipation-fluctuation (LDF) ratio R as the ratio of the local compressibility κ_i to local number fluctuations δn_i^2 at site i, defined by

$$\begin{aligned} R &= \kappa_i/\delta n_i^2 \\ \kappa_i &= \partial n_i/\partial \mu \\ \delta n_i^2 &= \langle \hat{n}_i^2 \rangle - \langle \hat{n}_i \rangle^2, \end{aligned} \tag{1}$$

where $n_i = \langle \hat{n}_i \rangle$ is the average density on site i.

Although other work has used the LDF ratio for thermometry [26, 28, 29], we go well beyond thermometry by exploiting its features to construct the full finite temperature phase diagram from the single quantity R.

We test our proposal on the 2D BHM using large-scale QMC simulations and show that remarkably, from the temperature dependence of this single quantity $R(T)$, it is possible to
(i) identify the onset of quantum effects T^*,
(ii) the crossover temperature T_Δ to the Mott phase,
(iii) the superfluid transition temperature T_c.

This allows us to determine the quantum critical region bounded by the temperature scales T^*, T_Δ and T_c. The

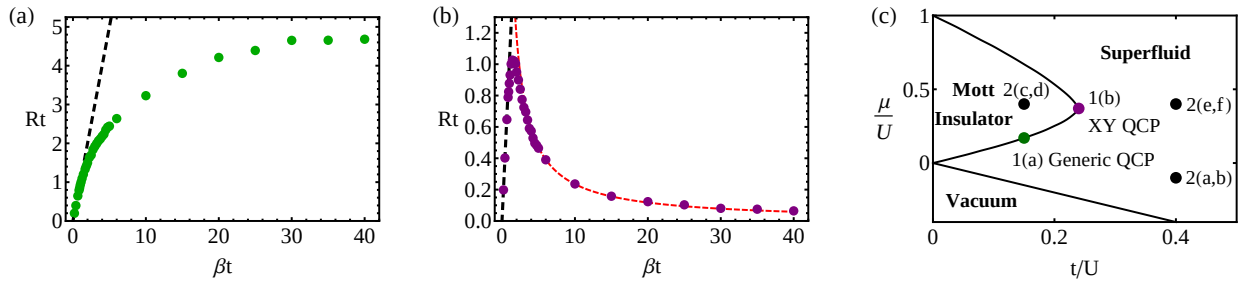

FIG. 1. (Color online) Identifying the Quantum Critical Region using Deviations from the Fluctuation Dissipation Theorem. (a) and (b) show the characteristic behavior of $R(T)$ obtained using QMC at a MF QCP and a 3D XY QCP, respectively, and clearly distinguishes between the two universality classes. At a MF QCP, the critical behavior of R is determined by the slow convergence of δn_i^2 and approaches a constant at low temperatures while at a 3D XY QCP, R's critical behavior is dominated by the compressibility's power law critical behavior, indicated by the dashed red line. The dashed black line is the high temperature behavior. Panel (c) shows the $T = 0$ phase diagram of the BHM with the parameters of each figure indicated.

thermodynamic and response functions in the quantum critical region should obey scaling based on exponents characteristic of the universality class of the QPT.

There are two universality classes of QCPs in the BHM at $T = 0$ in the chemical potential $\mu/U - t/U$ plane: a generic mean field (MF) QCP and the particle-hole symmetric QCP at the tip of the each Mott lobe in the 3D XY universality class[8]. We show that the universality class controlling the fluctuations in the quantum critical region can be deduced from the behavior of $R(T)$ (see Fig. 1). This is one of our central results.

There have been recent attempts to scale the experimental data for number fluctuations near a QCP, however, the error bars on the critical exponents are still rather large[27]. The coarse-grained analysis using $R(T)$ could serve as a precursor to scaling by identifying the scalable regime of the experimental data which may improve the error bars on the exponents.

This explicit demonstration of the utility of $R(T)$ within the BHM opens up the possibility of finding such phase diagrams for general quantum Hamiltonians *directly* from experimental data. We thus provide the crucial missing link in the grand challenge to emulate strongly correlated materials such as the high temperature superconductors using ultracold atoms in optical lattices[30].

The quantum fluctuation-dissipation theorem and $R(T)$ are discussed in section 2. In section 3, the BHM and generic properties of $R(T)$, including at high temperatures and at the onset of quantum effects, are described. Characteristic traces of $R(T)$ in the superfluid and Mott insulator states and extraction of T_c and T_Δ are described in section 4. Using $R(T)$, a finite temperature phase diagram is constructed and the quantum critical region is described in section 5 and finite size effects are discussed in section 6.

II. THE FLUCTUATION-DISSIPATION THEOREM

The quantum fluctuation-dissipation theorem (FDT) describes the response of a system defined by the Hamiltonian $\hat{H}$ to a perturbation coupled to an operator $\hat{A}$ within the system. It relates the imaginary part of the response function $\chi''(q,\omega)$ to the dynamic structure factor $S(q,\omega)$ at inverse temperature $\beta = 1/T$, wavevector q and frequency ω. In the following, we derive the quantum FDT and discuss the limiting cases of high temperature and of $[\hat{A},\hat{H}] = 0$ before turning to its application to ultracold atom systems and the LDF ratio $R(T)$.

Consider a quantum system of volume V defined by $\hat{H}$ with many body states and energies $\hat{H}|\Psi_n\rangle = \epsilon_n|\Psi_n\rangle$ that is perturbed by a probe $\hat{H}'(t)$. We assume that the external perturbation $F_A(t)$ couples to $\hat{A}$ via $\hat{H}'(t) = -\hat{A}F_A(t)$. For a spatially varying probe $\hat{H}'(t) = -\int d\mathbf{r}\hat{A}(\mathbf{r})F_A(\mathbf{r},t) = -\frac{1}{V}\sum_{\mathbf{q}}\hat{A}_{-\mathbf{q}}F_{\mathbf{q}}(t)$.

The response $\langle\hat{B}\rangle$ to linear order in the perturbation is $\langle\hat{B}\rangle(t) = \int_{-\infty}^{\infty}dt'\chi_{BA}(t-t')F_A(t')$ where $\chi_{BA}(t-t') = i\theta(t-t')\left\langle\left[\hat{B}(t),\hat{A}(t')\right]\right\rangle$. By using a spectral representation in terms of the exact eigenstates of $\hat{H}$ and the Heisenberg representation of the time dependent operators, we obtain

$$\chi_{BA}(\mathbf{q},\omega) = \frac{1}{V}\sum_{m,n}\frac{e^{-\beta\epsilon_m}}{\mathcal{Z}}\left[\frac{(A_{-\mathbf{q}})_{mn}(B_{\mathbf{q}})_{nm}}{\omega+i\eta+\epsilon_{nm}} - \frac{(B_{\mathbf{q}})_{mn}(A_{-\mathbf{q}})_{nm}}{\omega+i\eta-\epsilon_{nm}}\right] \quad (2)$$

where $\epsilon_{nm} = \epsilon_n - \epsilon_m$ and $\eta = 0^+$ is a small positive number to ensure convergence as $t \to \infty$. The well-known identity $\lim_{\eta\to 0^+}\frac{1}{x\pm i\eta} = P(\frac{1}{x}) \mp i\pi\delta(x)$ yields the imaginary part of the response function,

$$\chi''_{BA}(\mathbf{q},\omega) = \frac{\pi}{V}\sum_{m,n}\frac{e^{-\beta\omega_m}}{\mathcal{Z}}\left[(A_{-\mathbf{q}})_{mn}(B_{\mathbf{q}})_{nm}\delta(\omega-\epsilon_{nm}) - (B_{\mathbf{q}})_{mn}(A_{-\mathbf{q}})_{nm}\delta(\omega+\epsilon_{nm})\right]. \quad (3)$$

Next we consider the corresponding correlation function defined as

$$S_{BA}(\mathbf{r},t;\mathbf{r}',t') = \langle \hat{B}(\mathbf{r},t)\hat{A}(\mathbf{r}',t')\rangle \tag{4}$$

$$S_{BA}(\mathbf{q},t-t') = \frac{1}{V}\langle \hat{B}_{\mathbf{q}}(t)\hat{A}_{-\mathbf{q}}(t')\rangle \tag{5}$$

for a translationally invariant system. Within the spectral representation we obtain

$$S_{BA}(\mathbf{q},\omega) = \frac{2\pi}{V}\sum_{m,n}\frac{e^{-\beta\epsilon_m}}{\mathcal{Z}}(B_{\mathbf{q}})_{mn}(A_{-\mathbf{q}})_{nm}\delta(\omega-\epsilon_{nm}). \tag{6}$$

By exchanging the indices in the second term in Eq.3, we obtain the quantum FDT

$$\begin{aligned}\chi''_{BA}(\mathbf{q},\omega) =& \frac{\pi}{V}(1-e^{-\beta\omega}) \\ & \sum_{m,n}\frac{e^{-\beta\omega_m}}{\mathcal{Z}}(B_{\mathbf{q}})_{mn}(A_{-\mathbf{q}})_{nm}\delta(\omega-\omega_{nm}) \\ =& \frac{1-e^{-\beta\omega}}{2}S_{BA}(\mathbf{q},\omega).\end{aligned} \tag{7}$$

A. Static Structure Factor

The definition of the static structure factor is

$$\begin{aligned}S_{BA}(\mathbf{q}) \equiv S_{BA}(\mathbf{q},t=0) &= \int_{-\infty}^{\infty}\frac{d\omega}{2\pi}S_{BA}(\mathbf{q},\omega) \\ &= \int_{-\infty}^{\infty}\frac{d\omega}{2\pi}\frac{2}{1-e^{-\beta\omega}}\chi''_{BA}(\mathbf{q},\omega).\end{aligned} \tag{8}$$

Using the oddness property $\chi''_{BA}(-\omega) = -\chi''_{BA}(\omega)$ yields

$$S_{BA}(\mathbf{q}) = \frac{1}{V}\langle \hat{B}_{\mathbf{q}}\hat{A}_{-\mathbf{q}}\rangle = \int_0^{\infty}\frac{d\omega}{\pi}\coth\left(\frac{\beta\omega}{2}\right)\chi''_{BA}(\mathbf{q},\omega). \tag{9}$$

B. The High Temperature Limit of the Quantum FDT

At temperatures $k_BT \gg \hbar\omega$ larger than any characteristic frequencies of the system, $\coth\left(\frac{\beta\omega}{2}\right) \to 2/\beta\omega$ and the static structure factor reduces to

$$\begin{aligned}S_{BA}(\mathbf{q}) &= \frac{2}{\beta}\int_0^{\infty}\frac{d\omega}{\pi}\frac{\chi''_{BA}(\mathbf{q},\omega)}{\omega} \\ &= T\chi'_{BA}(\mathbf{q},\omega=0)\end{aligned} \tag{10}$$

where we have used the Kramers-Krönig relation $\chi'_{BA}(\mathbf{q},\omega) = P\int_{-\infty}^{\infty}\frac{d\omega'}{\pi}\frac{\chi''_{BA}(q,\omega')}{\omega'-\omega}$ to relate the real and imaginary parts of the response function. Since $\chi'' = 0$ when $\omega = 0$, we can replace χ' by simply χ.

C. The Quantum FDT for Conserved Quantities

We use (i) the definition of the correlation function for a conserved quantity, (ii) the quantum FDT, and (iii) the Kramers-Krönig relation to finally derive $\chi_{AA}(q\to 0,\omega=0) = \beta S_{AA}(q\to 0,t=0)$.

A conserved quantity $\hat{A}(\mathbf{q}=\mathbf{0}) \equiv \hat{A}_0$ such as the total number of particles $\hat{n}(\mathbf{q}=\mathbf{0}) = \sum_{\mathbf{k}}\hat{a}^{\dagger}_{\mathbf{k}}\hat{a}_{\mathbf{k}} = \hat{N}$, must commute with the Hamiltonian $\left[\hat{A}_0,\hat{H}\right] = 0$. This implies that the matrix element $\langle\Psi_m \mid \left[\hat{A}_0,\hat{H}\right] \mid \Psi_n\rangle = 0$ or equivalently $(\epsilon_n-\epsilon_m)(A_0)_{mn} = 0$. If $m\neq n$, we must have $(A_0)_{mn} = 0$ which results in

$$\begin{aligned}\lim_{\omega\to 0}\lim_{\mathbf{q}\to 0}\chi_{AA}(\mathbf{q},\omega) &= \lim_{\omega\to 0}\frac{2}{V}\sum_{m,n}\frac{e^{-\beta\epsilon_m}}{\mathcal{Z}}\left[\frac{\epsilon_{nm}\mid(A_0)_{mn}\mid^2}{(\omega+i\eta)^2-\epsilon_{nm}^2}\right] \\ &= 0\end{aligned} \tag{11}$$

using Eq. 2. Thus $\chi_{AA}(\mathbf{q}=0,\omega\to 0) = 0$ if A_0 is a conserved quantity.

However, reversing the order of the limits generally results in a finite result. For the case of a density perturbation,

$$\begin{aligned}\lim_{\mathbf{q}\to 0}\lim_{\omega\to 0}\chi_{AA}(\mathbf{q},\omega) &= \lim_{\mathbf{q}\to 0}\frac{2}{V}\sum_{m,n}\frac{e^{-\beta\epsilon_m}}{\mathcal{Z}}\left[\frac{\epsilon_{nm}\mid(A_{\mathbf{q}})_{mn}\mid^2}{(\omega+i\eta)^2-\epsilon_{nm}^2}\right] \\ &= n^2\kappa_T.\end{aligned} \tag{12}$$

The last equality in Eq. 12 follows from the perturbation $\hat{H}' = -\int d\mathbf{r}\delta\hat{n}(\mathbf{r})\delta\hat{\mu}(\mathbf{r},t) = -\frac{1}{V}\sum_{\mathbf{q}}\delta\hat{n}_{-\mathbf{q}}\delta\hat{\mu}_{\mathbf{q}}(t)$ which produces the response

$$\chi_{nn}(\mathbf{q}\to 0,\omega=0) = \frac{\langle\delta\hat{n}_{-\mathbf{q}\to 0}\rangle}{\delta\hat{\mu}_{\mathbf{q}\to 0}}(\omega=0) \tag{13}$$

$$= \left(\frac{\partial n}{\partial\mu}\right)_{T,V} = n^2\kappa_T \tag{14}$$

where κ_T is the isothermal compressibility and n is the average density.

Another way to understand the behavior of the quantum FDT for a conserved quantity $\hat{A}(\mathbf{q}=\mathbf{0},t)$ is to note that both it and the correlation $\hat{A}(\mathbf{q}=\mathbf{0},t)\hat{A}(-\mathbf{q}=0,t')$ are independent of t and t' and hence its Fourier transform must be a delta function in frequency. Thus from Eq. 5

$$S_{AA}(\mathbf{q}=0,\omega) = 2\pi\delta(\omega)S_{AA}(\mathbf{q}=0). \tag{15}$$

From the quantum FDT Eq. 7 we obtain for a conserved quantity with the correlation function Eq. 15,

$$\chi''_{AA}(\mathbf{q}=0,\omega) = (1-e^{-\beta\omega})\pi S_{AA}(\mathbf{q}=0)\delta(\omega). \tag{16}$$

By using the Kramers-Krönig relation we find

$$\begin{aligned}\chi_{AA}(\mathbf{q}=0,\omega\to 0) &= S_{AA}(\mathbf{q}=0)\int_{-\infty}^{\infty}d\omega\frac{1-e^{-\beta\omega}}{\omega}\delta(\omega) \\ &= \beta S_{AA}(\mathbf{q}=0) = \frac{\beta}{V}\langle\hat{A}_0^2\rangle\end{aligned} \tag{17}$$

and for particle number perturbations $\delta\hat{N} = \hat{N} - \langle\hat{N}\rangle$

$$\chi_{\delta N\delta N}(\mathbf{q}=0) = \frac{\beta}{V}\langle\delta\hat{N}^2(\mathbf{q}=0)\rangle = n^2\kappa_T. \quad (18)$$

We stress that while this result may look similar to the high temperature limit of Eq. 10, because the particle number is a conserved quantity it is valid even in the quantum regime.

D. Probing Trapped Ultracold Atoms

The pioneering *in situ* local density measurements narrows our focus to global number fluctuations $\delta N^2 = \langle\hat{N}^2\rangle - \langle\hat{N}\rangle^2$ and local number fluctuations $\delta n_i^2 = \langle\hat{n}_i^2\rangle - \langle\hat{n}_i\rangle^2$ at site i. For global number fluctuations, the $\omega = 0$ quantum FDT for commuting observables, with average density $n = \langle\hat{N}\rangle/V$ and isothermal compressibility κ_T, is

$$n^2\kappa_T = \frac{\partial n}{\partial\mu} = \beta\frac{\delta N^2}{V}\ . \quad (19)$$

While Eq. 19 resembles the classical FDT, it is crucial to note that it is valid at all temperatures.

There are two ways to probe the system locally. A local perturbation of the chemical potential by $\delta\mu_i$ at site i results in a local density variation δn_i. This procedure leads to the single site form of the classical FDT $\kappa_{i\,L} \equiv \frac{\partial n_i}{\partial\mu_i} = \beta\ \delta n_i^2$, and is only valid at high temperatures since the density on a given site is not conserved. Both this local relation and the global FDT of Eq. 19 can be used for thermometry [26, 28, 29], but their ability to reveal other properties of the system is severely limited.

We propose that the LDF ratio R defined in Eq. 1 is significantly more useful since it is sensitive to the nature of the phase and to various energy scales. The essential difference is that R involves $\kappa_i = \partial n_i/\partial\mu$ which measures the *local* density change in response to a *global* chemical potential μ variation, and as such is sensitive to long range order and phase transitions, in contrast to $\kappa_{i\,L}$ which is the local response to a local perturbation. Although we investigate R in a uniform system where $\kappa_i = n^2\kappa_T$, it is important to keep in mind its applicability to inhomogeneous systems like trapped atomic gases. Assuming the local density approximation, κ_i and R can be extracted directly from the density profile $n(\mu(r))$ [31] of ultracold atoms in a trap and the phase diagram of the homogeneous system, as a function of μ, can be constructed from $R(T)$.

E. The Ideal Gas

We describe the high temperature behavior of $R(T)$ by deriving the compressibility and number fluctuations of the ideal gas. From the equation of state $PV = Nk_BT$, we obtain

$$\kappa_T \equiv -\frac{1}{V}\left(\frac{\partial V}{\partial P}\right)_{T,N} \equiv \frac{1}{n^2}\frac{\partial n}{\partial\mu} = \frac{\beta}{n}. \quad (20)$$

For an ideal gas, the chemical potential is $\beta\mu = -\log\left(\frac{1}{n\lambda_T^d}\right)$, where the thermal deBroglie wavelength $\lambda_T = h/\sqrt{2\pi mk_BT}$. For fixed μ, the high temperature expansion of the density $n(\mu, T)$ is

$$n = \frac{e^{\beta\mu}}{\lambda_T^d} \sim T^{d/2}\left(1 + \frac{\mu}{k_BT} + \frac{1}{2}\left(\frac{\mu}{k_BT}\right)^2\right), \quad (21)$$

which implies that the temperature dependence of the local compressibility is

$$n^2\kappa_T = \frac{\partial n}{\partial\mu} \sim T^{d/2-1}\left(1 + \frac{\mu}{k_BT}\right). \quad (22)$$

Using the FDT at high temperatures, we find

$$\delta n^2 \approx \frac{\partial n}{\partial\mu}T \sim T^{d/2}\left(1 + \frac{\mu}{k_BT}\right). \quad (23)$$

Thus, we find that in uniform 2D ideal gas the local compressibility $\kappa_i = n^2\kappa_T$ is independent of temperature and the number fluctuations δn^2 scale linearly with T. The ratio $R = \kappa_i/\delta n^2 = n^2\kappa_T/\delta n^2$ is linear in T^{-1} as dictated by the FDT and observed in Fig.2(a,b). Only when quantum effects become important does R exhibit non-trivial behavior.

III. $R(T)$ IN THE BOSE HUBBARD MODEL

In the following, we demonstrate the potential for R to map out finite temperature phase diagrams by evaluating R in the BHM. Bosons trapped in an optical lattice and confined in a potential are described by

$$\hat{H} = -\frac{t}{z}\sum_{\langle i,j\rangle}(\hat{a}_i^\dagger\hat{a}_j + \hat{a}_i\hat{a}_j^\dagger) + \frac{U}{2}\sum_i\hat{n}_i(\hat{n}_i - 1) - \sum_i\mu_i\hat{n}_i. \quad (24)$$

Here $\hat{a}_i$ ($\hat{a}_i^\dagger$) are boson annihilation (creation) operators, $\langle\ldots\rangle$ indicates nearest neighbor sites, $\mu_i = \mu_0 - \alpha r_i^2$ is the chemical potential on site i for a parabolic confining potential, and t and U set the hopping and interaction energy scales, respectively. We simulate the BHM at finite temperatures with worldline quantum Monte Carlo (QMC) using the directed loop algorithm on up to 64^2 site lattices [13, 32]. We establish the essential ideas in a uniform system ($\alpha = 0$) for clarity, but the results are easily extended to the nonuniform system by using the local density approximation[33].

IV. QUANTUM PHASES

A. Classical Regime

At high temperatures, $T \gg U \gg t$, the system is in a non-interacting classical regime. As in the ideal gas,

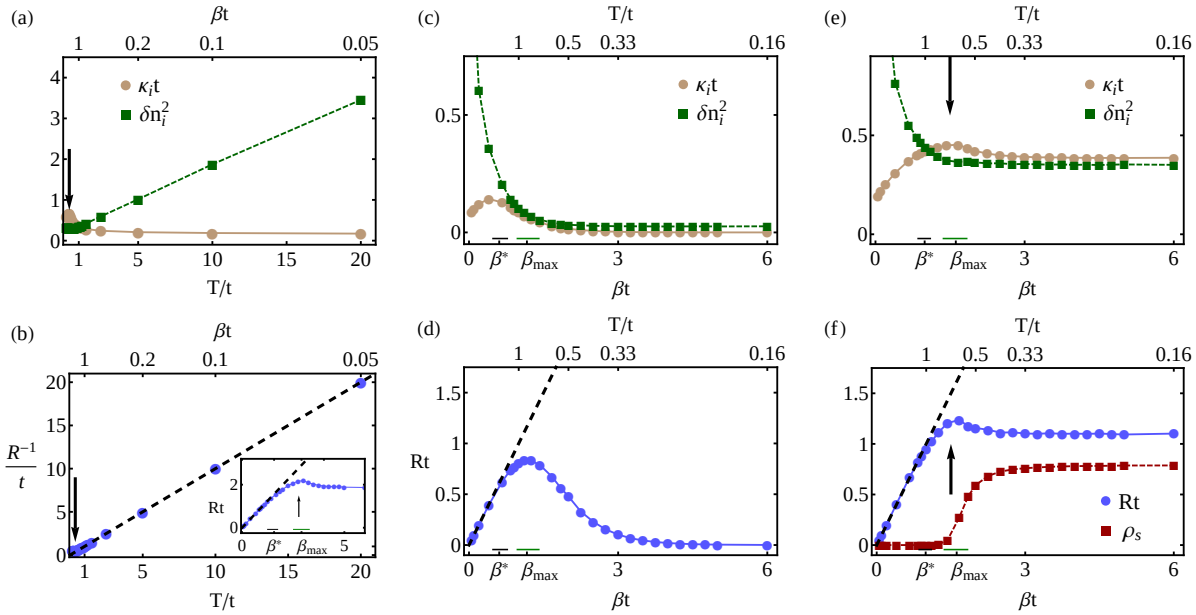

FIG. 2. (Color online) Temperature Scales Encoded in R. Panels (a) and (b): High temperature behavior of compressibility κ_i (circles) and number fluctuations δn_i^2 (squares) demonstrates that the LDF $R = \kappa_i/\delta n_i^2$ is determined by δn_i^2. The inset in (b) replots the data as $R(\beta)$ to exhibit the low temperature behavior. Panels (c) and (d): In the MI, κ_i is exponentially suppressed as $T \to 0$ while local quantum fluctuations maintain δn_i^2 at a finite value. The corresponding LDF R in the MI shows a characteristic maximum near T_Δ and decays exponentially at low T. Panels (e) and (f): In the SF, κ_i, δn_i^2 and R all approach a finite constant as $T \to 0$. The peak in R occurs at β_{max} and agrees well with the inverse superfluid T_c (indicated by the arrow) obtained from the superfluid density ρ_s (squares in (f)). In all panels, the inverse temperature β^* indicates when R deviates from the classical limit and is estimated from $R(\beta^*)/\beta^* = 0.95$. The dashed black line indicates the high temperature $R \approx \beta$ limit in (b,d,f) and horizontal bars indicate uncertainty in β^* and β_{max}.

the inverse LDF ratio $R^{-1} \approx T$ behavior is governed by the density fluctuations δn_i^2, which increase linearly with temperature (κ_i remains finite and independent of T). As T decreases to the regime $U \gg T \gg t$, the system remains classical. Interaction effects cause both κ_i and δn_i^2 to deviate from the high-T ideal gas limit but the inverse LDF ratio remains approximately linear in T (see Fig. 2(a,b)).

The quantity $R(T)$ can also be used to test for equilibration of the system in different regions in a trap. For bosons in optical lattices, the Mott-like center is sometimes observed to be at a significantly different temperature from the superfluid or normal wings [18–21]. In such situations, successive local measurements of R can be useful to garner information about rate-limiting processes for achieving equilibrium.

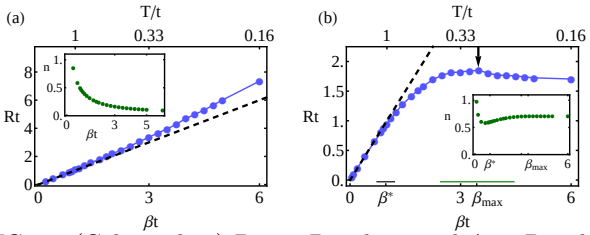

FIG. 3. (Color online) Boson Bunching and Anti-Bunching. Panel (a) shows bunching ($R > \beta$) at low temperatures for $t/U = 1.0$, $\mu/U = -0.95$. This system is not superfluid at the temperatures probed. Panel (b) shows anti-bunching ($R < \beta$) at low temperatures for $t/U = 0.15$, $\mu/U = 0.05$ and the error in β^* is indicated by the horizontal bar. The large error in β_{max} (horizontal bar) is characteristic of the superfluid in the presence of strong interactions, where the peak in R is difficult to resolve. The inset in each panel shows the density for the same parameters.

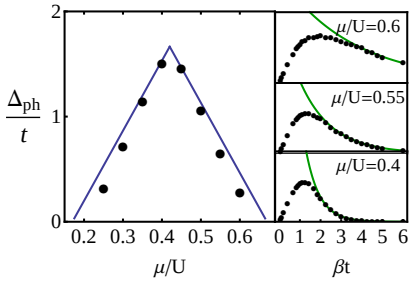

FIG. 4. (Color online) Extracting the Particle-Hole Gap from R. The righthand column shows $R(T)$ (circles) at $t/U = 0.15$ and for several μ/U values as well as the exponential fit to extract Δ_{ph} (solid line). The lefthand plot shows the extracted Δ_{ph} (circles) and the results from $T = 0$ QMC calculations by Capogrosso-Sansone, *et al*[34] (solid line).

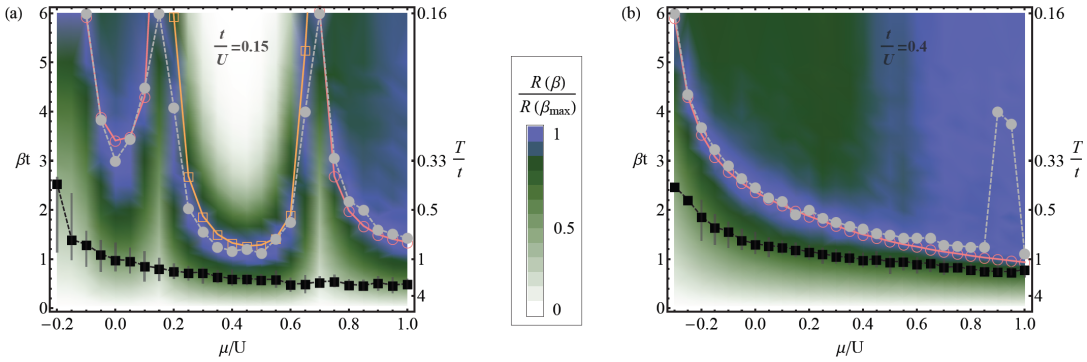

FIG. 5. (Color online) Determination of the Phase Diagram of a Quantum Hamiltonian using Local Observables: This figure shows the density plot of LDF ratio R in the inverse temperature-chemical potential $(\beta t - \mu/U)$ plane at (a) $t/U = 0.15$ and (b) $t/U = 0.4$. We determine the phase diagram from $R(\beta)$ by marking two inverse temperature scales, $\beta^* = 1/T^*$ (solid black squares) that indicates the onset of quantum effects, and $\beta_{max} = 1/T_{max}$ (solid grey circles) that delineate phase transitions or crossovers. β_{max} agrees with the characteristic temperature scales in the superfluid $1/T_c$ (open red circles) and the MI phases $1/T_\Delta$ (open orange squares). These are calculated independently of R by examining ρ_s ($\rho_s(T_c) = 0.1$) and κ_i ($\kappa_i(T_\Delta)t = 0.05$). To highlight the peak at $R(\beta_{max})$, the density color scheme is normalized so that $R(\beta_{max}) = 1$ for each value of μ.

B. Onset of Quantum Effects T^*

The deviation of R^{-1} from linear T behavior defines the temperature T^* at which quantum effects first become evident. In Ref. [35], such deviations have been observed for a continuum system near the normal-superfluid transition. The exact formula

$$R = \frac{\kappa_i}{\delta n_i^2} = \beta \left(1 + \frac{\sum_{i \neq j} \left(\langle \hat{n}_i \hat{n}_j \rangle - \langle \hat{n}_i \rangle \langle \hat{n}_j \rangle \right)}{V \delta n_i^2} \right) \qquad (25)$$

illustrates that any deviation of R from β is due to inter-site density fluctuation correlations. At low density $n \lesssim 0.1$ and small interactions U, the quantum statistics of bosons leads to bunching (Fig. 3(a)), or positively correlated density fluctuations, and manifests as $R > \beta$. For larger density and stronger interaction, the inter-boson repulsion overwhelms the bosonic tendency to bunch and density fluctuations between sites become anticorrelated, causing $R < \beta$ (Fig. 3(b)).

Understanding the behavior of κ_i and δn_i^2, the observables composing the LDF ratio, is essential for understanding the signatures of the phases in R (see Fig. 2 for typical MI and SF systems). The peak in R at a temperature T_{max} is a generic feature of the system entering an ordered phase.

C. Mott Insulator T_Δ

The Mott gap suppresses the low energy excitations contributing to the compressibility, causing κ_i to vanish exponentially with the $T = 0$ energy gap to add a particle or a hole, whichever is smaller [8], as $T \to 0$. The energy gap extracted by fitting a decaying exponential to κ_i or R agrees very well with QMC simulations [34] deep in the MI (Fig. 4), but differ on approaching QCPs, which we attribute mainly to finite temperature and size effects. On the other hand, in spite of the Mott gap, the local number fluctuations remain finite down to the lowest temperatures due to local quantum fluctuations.

With increasing temperature, the MI crosses over into the normal state with no transition and therefore shows no specific signature in κ_i, so the peaks of R and κ_i do not necessarily line up, as in Figs. 2(c,d). We identify the temperature T_{max} of the peak in R with the MI crossover temperature T_Δ as confirmed by QMC simulations, where T_Δ is somewhat arbitrarily defined by a vanishingly small compressibility.

D. Superfluid T_c

The gapless collective excitations in the SF cause both κ_i and δn_i^2 to approach a constant value as $T \to 0$. As the system condenses at T_c, critical fluctuations lead to a peak or singularity in κ_i described by the BKT universality class for the normal-SF transition. Since the appearance of quasi-long-range phase coherence below T_c does not affect the smoothly decreasing local δn_i^2, the peak in R mirrors the peak in κ_i near T_c and is shown in Figs. 2(e,f). Comparison with the SF T_c calculated by the vanishing the superfluid density, confirms that $T_{max} \approx T_c$, illustrated in Fig. 2(f).

V. CRITICAL REGIME

The degeneracy temperature T^* depends on t/U and μ/U and is independent of the underlying critical points. This is illustrated for $t/U = 0.15$ and $T = 0$ in Fig. 5(a) where the system progresses from vacuum to SF, then hits the two QCPs bounding the $n = 1$ MI and returns to SF as μ/U increases. In the temperature range between T^* and T_{max}, the system is quantum critical and

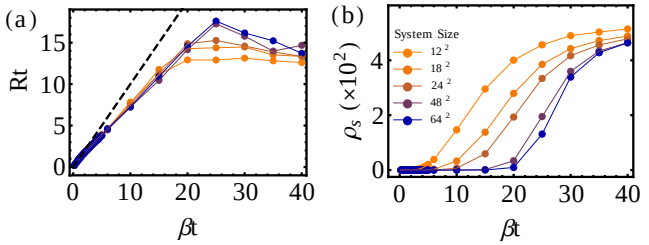

FIG. 6. (Color online) Finite Size Effects at the Superfluid-Normal Transition at $t/U = 0.08$ and $\mu/U = 0.08$. We observe significant finite size effects in $R(T)$ (a) and superfluid density ρ_s (b). As the system size increases, the peak in $R(T)$ becomes more pronounced and the system becomes less superfluid at a given temperature. The finite size effects are smaller for a system further from the QCP at $\mu/U \simeq 0.084$.

thermodynamic observables scale according to the universality class of the underlying QCP.

At the superfluid-normal finite temperature transition far from QCPs, the narrowing quantum critical region reflects a shift to classical criticality. This is seen at large μ in Fig. 5(a) and in Fig. 5(b) for $t/U = 0.4$, where the proximity of the Mott lobe tipe at $t/U \approx 0.24$ opens a window of quantum critical fluctuations at intermediate densities. The smaller region of quantum critical fluctuations significantly shrinks the peak in κ_i and R at the SF-normal phase transition and makes accurate identification of T_{max} difficult, as seen for both t/U values. We use T^*, T_Δ and T_c to identify the quantum critical region and propose that it is only appropriate to use temperatures within this range for scaling analyses.

Furthermore, R distinguishes between the MF and 3D XY QCPs in the BHM. Note that δn_i^2 is local and does not exhibit any critical scaling while the compressibility scales like $\kappa_i \sim \beta^{1-d/z}$ at the critical point, where d is the spatial dimension and z is the dynamical exponent [8]. At the 3D XY QCP, $z = 1$ and both κ_i and R decay according to the power law $\kappa_i \sim \beta^{-1}$, shown in Fig. 1(b). Since $z = 2$ at the MF QCP, κ_i is independent of temperature in the critical regime. In sufficiently large systems, the slow decay of δn_i^2 to its final value dictates the behavior of R at the MF QCP, shown in Fig. 1(a).

VI. FINITE SIZE EFFECTS

Finite size effects are briefly studied in the vicinity of and directly at MF quantum critical points. In both cases, the observables that probe long range correlations (κ_i, ρ_s and R) exhibit large finite size effects while the local number fluctuations δn_i^2 are unaffected by the system size L. The superfluid-normal finite temperature transition (see Fig. 6(b)) is in the Berezinski-Kosterlitz-Thouless universality class, so both κ_i and R are cusplike rather than singular at the transition. This cusp or peak becomes more pronounced in larger systems, as shown in Fig. 6(a). Increasing L significantly suppresses both T_c and ρ_s (see Fig. 6(b)), partly because of the nearby MF quantum critical point.

The finite size effects change slightly at the MF quantum critical point. As expected, $\rho_s \to 0$ as L increases while δn_i^2 is unchanged, shown in Fig. 7. For sufficiently large systems, the compressibility κ_i converges to a constant at small temperatures. At a MF QCP and for sufficiently large L, the LDF ratio $R(T)$ is dominated by δn_i^2 at low temperatures and monotonically increases to a finite value, in stark contrast to its behavior at the BKT transition (Fig. 6(a)) or at the 3D XY QCP (Fig. 1(b)).

In conclusion, while both $\partial N/\partial\mu = \beta\ \delta N^2$ and $\partial n_i/\partial\mu_i = \beta\ \delta n_i^2$ FDT are exact relations useful for estimating the temperature, we construct a LDF ratio R and show that it is sensitive to far more than just the temperature. With R, the SF and MI states can be identified and the finite temperature phase diagram can be mapped without the need for QMC simulations and with a single, experimentally accessible quantity. A corollary is the identification of the temperature scales (T^*, T_c and T_Δ) that bound the quantum critical region and the ability to distinguish between the MF and 3D XY universality classes using only R. It is possible to generalize R to two-component systems as well as to disordered systems and also probe spin susceptibility and corresponding spin fluctuations for magnetic systems. Given the very fundamental basis on which the LDF ratio is constructed, we expect it to be an ideal candidate for probing phases and quantum criticality of general quantum Hamiltonians.

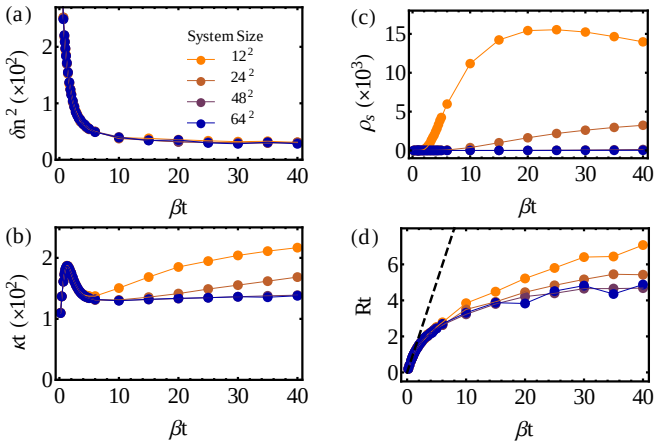

FIG. 7. (Color online) Finite Size Effects at the Mean Field Quantum Critical Point at $t/U = 0.15$ and $\mu/U = 0.172$. The local number fluctuations δn_i^2 (a) do not depend on the system size. The long-range observables like the compressibility κ_i (b), superfluid density ρ_s (c) and R (d) do vary with the system size before converging for 48^2 and 64^2 site systems. Due to simulation time limitations, the error for the 64^2 site system is larger than for the other system sizes.

Acknowledgments

This work was financially supported by the NSF DMR-0907275 and ICAM (ED and NT) and the DARPA OLE program.

[1] T. Esslinger, Annual Review of Condensed Matter Physics **1**, 129 (2010).

[2] J. K. Chin, D. E. Miller, Y. Liu, C. Stan, W. Setiawan, C. Sanner, K. Xu, and W. Ketterle, Nature **443**, 961 (2006).

[3] R. Jordens, N. Strohmaier, K. Gunter, H. Moritz, and T. Esslinger, Nature **455**, 204 (2008).

[4] U. Schneider, L. Hackermüller, S. Will, T. Best, I. Bloch, T. A. Costi, R. W. Helmes, D. Rasch, and A. Rosch, Science **322**, 1520 (2008).

[5] T. Paiva, R. Scalettar, M. Randeria, and N. Trivedi, Phys. Rev. Lett. **104**, 066406 (2010).

[6] S. Fuchs, E. Gull, L. Pollet, E. Burovski, E. Kozik, T. Pruschke, and M. Troyer, Phys. Rev. Lett. **106**, 030401 (2011).

[7] T. Paiva, Y. L. Loh, M. Randeria, R. T. Scalettar, and N. Trivedi, Phys. Rev. Lett. **107**, 086401 (2011).

[8] M. P. A. Fisher, P. B. Weichman, G. Grinstein, and D. S. Fisher, Physical Review B **40**, 546 (1989).

[9] M. Greiner, O. Mandel, T. Esslinger, T. W. Hansch, and I. Bloch, Nature **415**, 39 (2002).

[10] D. Jaksch, C. Bruder, J. I. Cirac, C. W. Gardiner, and P. Zoller, Phys. Rev. Lett. **81**, 3108 (1998).

[11] S. Sachdev, *Quantum Phase Transitions*, 2nd ed. (Cambridge University Press, 2011).

[12] R. B. Diener, Q. Zhou, H. Zhai, and T.-L. Ho, Physical Review Letters **98**, 180404 (2007).

[13] Y. Kato, Q. Zhou, N. Kawashima, and N. Trivedi, Nat Phys **4**, 617 (2008).

[14] S. Trotzky, L. Pollet, F. Gerbier, U. Schnorrberger, I. Bloch, N. V. Prokof'ev, B. Svistunov, and M. Troyer, Nat Phys **6**, 998 (2010).

[15] X. Du, S. Wan, E. Yesilada, C. Ryu, D. J. Heinzen, Z. Liang, and B. Wu, New Journal of Physics **12**, 083025 (2010).

[16] R. Grimm, in *Proceedings of the International School of Physics "Enrico Fermi," Course CLXIV*, edited by M. Inguscio, W. Ketterle, and C. Salomon (IOS Press, 2006).

[17] F. Gerbier, S. Fölling, A. Widera, O. Mandel, and I. Bloch, Phys. Rev. Lett. **96**, 090401 (2006).

[18] C.-L. Hung, X. Zhang, N. Gemelke, and C. Chin, Phys. Rev. Lett. **104**, 160403 (2010).

[19] W. S. Bakr, A. Peng, M. E. Tai, R. Ma, J. Simon, J. I. Gillen, S. Fölling, L. Pollet, and M. Greiner, Science **329**, 547 (2010).

[20] J. F. Sherson, C. Weitenberg, M. Endres, M. Cheneau, I. Bloch, and S. Kuhr, Nature **467**, 68 (2010).

[21] S. S. Natu, K. R. A. Hazzard, and E. J. Mueller, Phys. Rev. Lett. **106**, 125301 (2011).

[22] W. S. Bakr, J. I. Gillen, A. Peng, S. Fölling, and M. Greiner, Nature **462**, 74 (2009).

[23] N. Gemelke, X. Zhang, C. Hung, and C. Chin, Nature **460**, 995 (2009).

[24] Q. Zhou and T.-L. Ho, Phys. Rev. Lett. **105**, 245702 (2010).

[25] K. R. A. Hazzard and E. J. Mueller, Phys. Rev. A **84**, 013604 (2011).

[26] S. Fang, C.-M. Chung, P. N. Ma, P. Chen, and D.-W. Wang, Physical Review A **83**, 031605 (2011).

[27] X. Zhang, C. Hung, S. Tung, and C. Chin, Science **335**, 1070 (2012).

[28] P. N. Ma, L. Pollet, and M. Troyer, Physical Review A **82**, 033627 (2010).

[29] Q. Zhou and T.-L. Ho, Phys. Rev. Lett. **106**, 225301 (2011).

[30] P. W. Anderson, P. A. Lee, M. Randeria, T. M. Rice, N. Trivedi, and F. C. Zhang, Journal of Physics: Condensed Matter **16**, R755 (2004).

[31] Q. Zhou, Y. Kato, N. Kawashima, and N. Trivedi, Physical Review Letters **103**, 085701 (2009).

[32] Y. Kato and N. Kawashima, Physical Review E **79**, 021104 (2009).

[33] K. W. Mahmud, E. N. Duchon, Y. Kato, N. Kawashima, R. T. Scalettar, and N. Trivedi, Phys. Rev. B **84**, 054302 (2011).

[34] B. Capogrosso-Sansone, S. G. Söyler, N. Prokof'ev, and B. Svistunov, Physical Review A **77**, 015602 (2008).

[35] C. Hung, X. Zhang, N. Gemelke, and C. Chin, Nature **470**, 236 (2011).